Improvement of signal propagation in the optoelectronic artificial spiking neuron by vibrational resonance

V. N. Chizhevsky* and M. V. Lakhmitski
B. I. Stepanov Institute of Physics, National Academy of Sciences of Belarus, 220072 Minsk, Belarus

(Received 10 July 2023; accepted 4 December 2023; published 8 January 2024)

Experimental evidence of vibrational resonance (VR) in the optoelectronic artificial spiking neuron based on a single photon avalanche diode and a vertical cavity laser driven by two periodic signals with low and high frequencies is reported. It is shown that a very weak subthreshold low-frequency (LF) periodic signal can be greatly amplified by the additional high-frequency (HF) signal. The phenomenon shows up as a nonmonotonic resonant dependence of the LF response on the amplitude of the HF signal. Simultaneously, a strong resonant rise of the signal-to-noise ratio is also observed. In addition, for the characterization of VR an area under the first LF period in the probability density function of interspike intervals for the LF signal and the maximal amplitude in this area were used, both of which also demonstrate a resonant behavior depending on the amplitude of the HF signal.

DOI: 10.1103/PhysRevE.109.014211

I. INTRODUCTION

In the last years there has been increasing interest in the phenomenon of vibrational resonance (VR) occurring in nonlinear systems, which was first demonstrated numerically in bistable systems by Landa and McClintock [1]. The phenomenon of VR shows up as resonant behavior at the frequency of the low-frequency (LF) input signal depending on the amplitude or frequency of the additional high-frequency (HF) excitation. In a sense VR is a deterministic analog of the phenomenon of stochastic resonance [2,3] where noise is replaced by a HF signal. First, VR has been evidenced experimentally in analog electronic circuits [4–6] and in a bistable vertical-cavity surface-emitting laser (VCSEL) for symmetrical and asymmetrical configurations of bistability in a VCSEL [7,8]. By now the phenomenon of VR, along with analog electronic circuits and VCSELs, was revealed experimentally in such diverse systems as an optical lattice [9], mechanical systems [10], a driven nanoelectromechanical nonlinear resonator [11], and a thermo-optic optomechanical nanocavity [12]. At the same time theoretical investigations demonstrated an occurrence of VR, for instance, in quantum systems [13–15], a Rayleigh-Plesset bubble oscillator [16], a parametrically excited gyroscope [17], groundwater-dependent plant ecosystems [18], time-delayed systems [19], a ferroelectric liquid crystal [20], in the perception of noisy images in the threshold detector [21], a three-level atomic optical bistable system [22], and in a number of theoretical models.

A number of papers were devoted to theoretical investigations of VR in single neuron models and neural networks of a different topology. In particular, VR was studied in a FitzHugh-Nagumo (FHN) model [23–25], coupled FHN neuron populations with different topologies [24], a neural feedforward network of FHN neurons [26], a network constructed by the Izhikevich neuron model [27], single and small-world networks of Hodgkin-Huxley neurons [25,28], and Hindmarsh-Rose neuronal systems [29].

Along with the theoretical studies of VR in the FHN model, an electronic neural circuit exactly ruled by FitzHugh-Nagumo equations was built to study experimentally the phenomenon of VR as well as the effect of noise on VR [30,31]. The propagation enhancement of low-frequency information in the network of these FHN electronic neurons depending on the applied additional HF signal was also studied [32,33].

Here, we present experimental evidence of the phenomenon of VR in an optoelectronic artificial spiking neuron (ASN) which is based on a single photon avalanche diode operating in the Geiger mode and a VCSEL [34]. This type of ASN mimics well the basic properties of biological neurons, such as the existence of a threshold and refractory period, an insensitivity to the effect of the stimuli strength above the threshold, and the dependence of the neuron fire rate to the stimuli strength. We here demonstrate that a weak subthreshold low-frequency periodic signal can be greatly enhanced by an additional high-frequency periodic signal with an optimal amplitude. At the same time this amplification is followed by a strong resonant rise of the signal-to-noise ratio (SNR). This means that we obtain simultaneously the signal amplification and a SNR gain larger the unity, which is important from a practical standpoint. It should be noted that the peculiarity of the effect of the periodic excitation in this ASN is that the subthreshold LF periodic signal does not induce any response until the LF amplitude reaches the laser threshold. Along with standard measures of VR as a response amplitude and SNR at the frequency of the LF signal, we used also for the characterization of VR such quantities as an area under the first LF period in the probability density function of interspike

*vnc@dragon.bas-net.by

 ©2024 American Physical Society

intervals (ISIs) for the LF signal and the maximal amplitude in this area. Both measures pass though the maximum similarly to the response amplitude at the frequency of the LF signal.

II. EXPERIMENTAL SETUP

An experimental study was performed with an optoelectronic artificial spiking neuron proposed in Ref. [34]. The artificial neuron is composed of a VCSEL, a variable optical attenuator (VOA), and a single photon avalanche diode (SPAD). A 850-nm VCSEL was used in the experiments. The temperature of the laser diode was controlled to within 0.01 °C. Two sine-wave/square-wave LF and HF periodic signals from an arbitrary function generator with frequencies $f_L = 100\,\text{kHz}$ and $f_H = 2\,\text{MHz}$ and different amplitudes A_L and A_H were directly applied to the laser diode. The amplitudes of periodical signals deviated from zero with mean values of $A_L/2$ and $A_H/2$, respectively. Both signal periods are significantly higher than the SPAD deadtime (≈45 ns). Here, the amplitude of the HF signal A_H is a control parameter. The amplitudes of both periodic signals were controlled from a computer. We have used a commercial SPAD (id100-MMF50, idQuantique) operating in a free-running mode with an active quenching circuit integrated with an avalanche diode. The detector has a dark count rate of 32 Hz and a deadtime of about 45 ns. The output pulse of the detector has a duration of about 10 ns and an amplitude of 2 V. The temporal responses of the ASN were detected by a USB oscilloscope with a sampling frequency up to 500 MHz and an input bandwidth of 250 MHz. Before considering the experimental results some remarks on the ASN operation peculiarities should be made. The character of the temporal response of the ASN to the effect of the long duration laser pulse (much longer than the SPAD deadtime) depends on its amplitude. For a weak pulse amplitude the ASN response has a series of stochastically distributed short pulses during the action of the excitation pulses. With increasing the excitation pulse amplitude the ASN response tends to a periodical character with the period determined by the SPAD deadtime [34]. The second peculiarity is that the photon detection probability depends on the laser wavelength. For the VCSEL used here in the experimental studies this probability is about 3%. Therefore we have an ASN with a probabilistic response where the detection probability depends on the pulse laser amplitude. In addition, there is also the laser threshold for injection current pulses applied to the laser.

III. TEMPORAL BEHAVOUR OF ASN WITH BEHARMONIC MODULATION

Figure 1 shows the temporal responses of the ASN for different values of the amplitude of the control signal A_H applied to the laser diode with a fixed value of the amplitude of the input LF signal $A_L = 0.2\,\text{V}$. Both LF and HF signals in Fig. 1 have square-wave shapes. The amplitude A_L is significantly less than the laser threshold which is about 1.845 V in the regime of the continuous dc current injection. In the absence of a control signal the ASN response demonstrates very rare single pulses corresponding mainly to the SPAD dark pulses [Fig. 1(a)]. When the additional modulation with

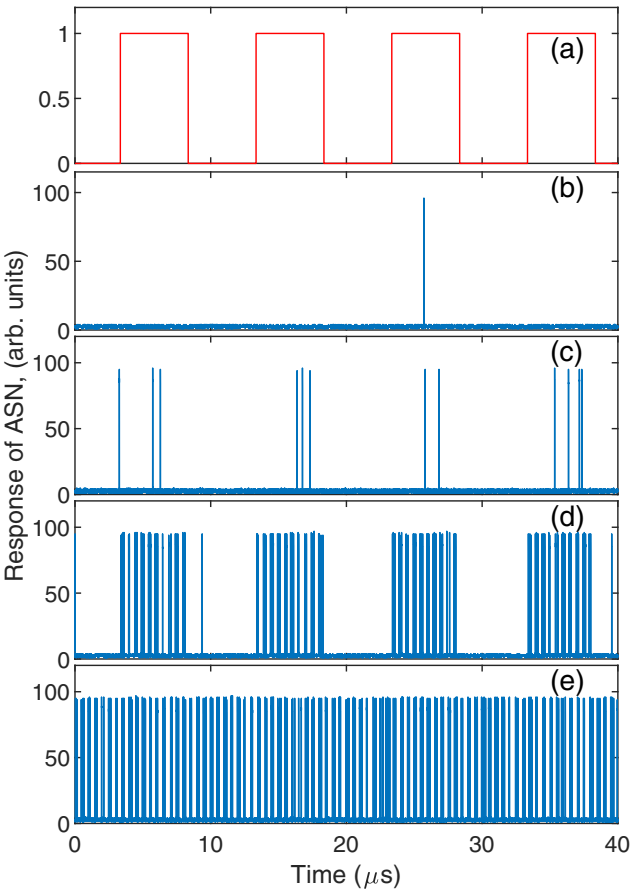

FIG. 1. Temporal responses of the ASN to the effect of the LF periodic square-wave modulation shown for different values of the HF control amplitude A_H. (a) LF modulation signal, $A_L = 0.2$ V; (b) $A_H = 0$, (c) 1.67, (d) 1.84, and (e) 1.94 V.

$A_H = 1.67\,\text{V}$ was added to the laser diode, one can see an appearance of the periodical response with irregular pulses within the semiperiods of the LF signal. A further increase of the amplitude A_H results in the appearance of pulse bursts going with the frequency of the LF modulation. Comparing this signal [Fig. 1(d)] with the input LF signal [Fig. 1(a)] one can note a perfect synchronization between them. Finally, for a large enough amplitude $A_H = 1.94\,\text{V}$, pulse packets going

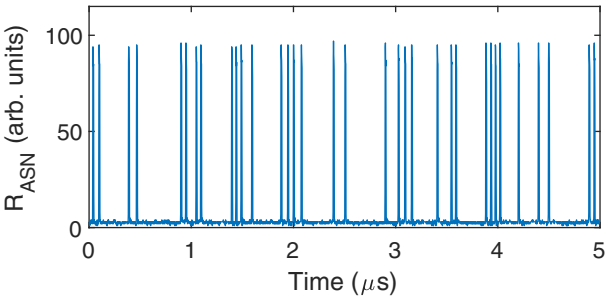

FIG. 2. Pulse trains of the response ASN R_{ASN} to the effect of the LF periodic square-wave modulation for $A_L = 0.2\,\text{V}$ and $A_H = 1.94\,\text{V}$ showing a stochastic appearance of spikes in each semiperiod of the HF modulation.

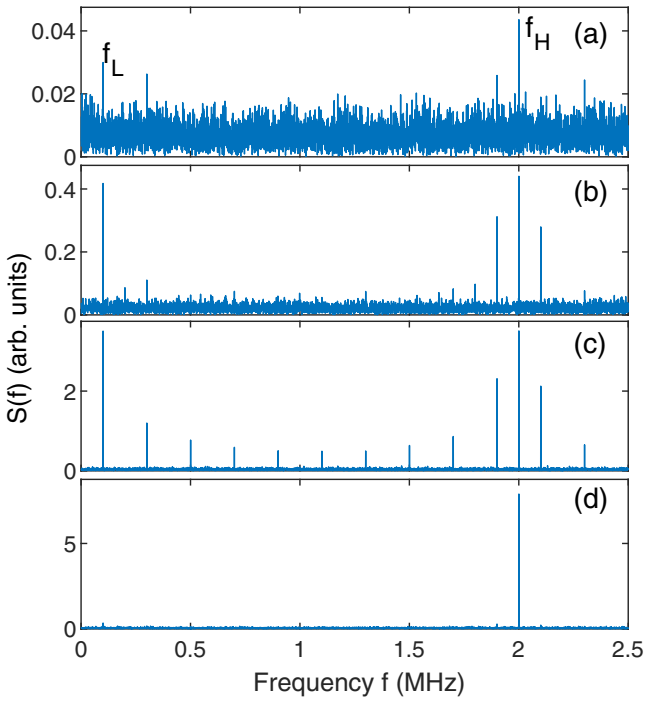

FIG. 3. Spectra of the ASN responses for different values of the control amplitude A_H. (a) $A_H = 1.65$, (b) 1.67, (c) 1.79, and (d) 2.04 V; $A_L = 0.2$ V.

with the frequency of the HF signal are observed. Such a series of pulse packets within a single semiperiod of the LF signal is shown in Fig. 2. Since the frequency ratio of the LF and HF signals is equal to 20, therefore the number of packets is ten. In this case each packet contains from one to five pulses which appear occasionally in each semiperiod of the HF signal. The maximal number of pulses is determined by the ratio between the semiperiod of the square-wave HF signal and the SPAD deadtime (45 ns). In this case the number of pulses is equal to five.

IV. SIGNAL AMPLIFICATION BY VR

As a rule, in experimental studies VR is characterized quantitatively by the response amplitude of the system at a low frequency which is obtained from the Fourier spectra of the time series. Figure 3 shows the amplitude spectra of the ASN for different values of the amplitude of the control signal A_H for the case when both periodical signals have a rectangular shape. One can see that the response at the frequency f_L increases as the A_H increases and then completely disappears beginning with a certain value of the amplitude A_H [Fig. 3(d)]. Figure 4 summarizes the results of the systematic study of the LF response of ASN depending on the amplitude of the additional HF signal for different values of A_L. The response amplitudes R_L and R_H were evaluated as the height of the peaks in the spectra at frequencies f_L and f_H, respectively.

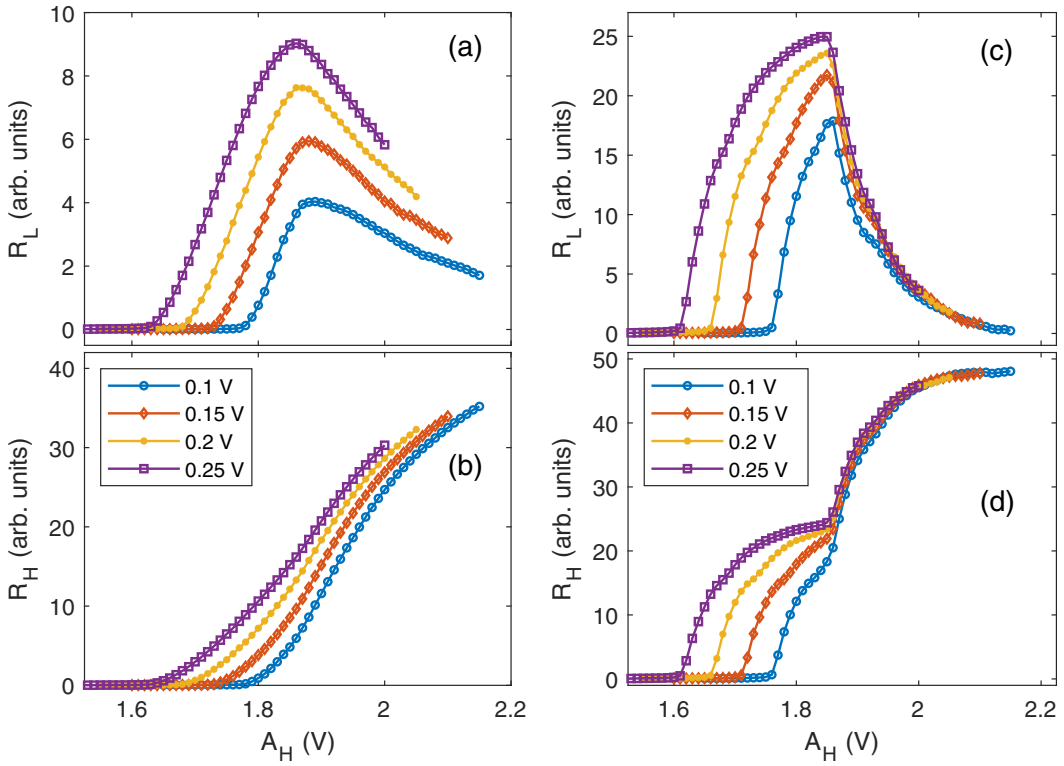

FIG. 4. Response of the ASN at frequencies f_L and f_H for sine-wave periodical signals (left panel) and square-wave signals [(c) and (d)] (right panel), respectively. The amplitudes A_L are the same for both types of LF signals. $A_L = 0.1$ (open circle), 0.15 (diamond), 0.2 (point), and 0.25 (square) V. All LF signal amplitudes are significantly below the laser threshold.

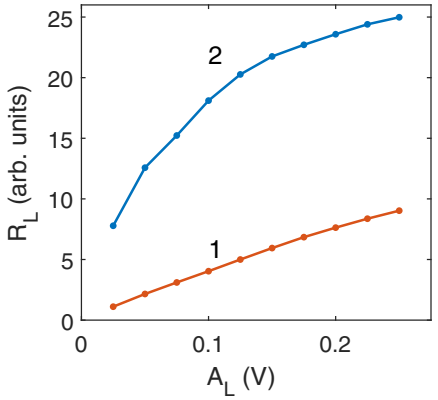

FIG. 5. Maximal values $R_L^{\max}$ of the LF response as a function of the LF amplitude for sine-wave (1) and square-wave (2) LF signals.

We used two types of periodic signals, namely, sine-wave and square-wave ones. Figures 4(a) and 4(c) show the response amplitude R_L as a function of the amplitude of the HF control signal for sine-wave and square-wave signals, respectively. Both figures clearly demonstrate a typical behavior of the response amplitude R_L depending on the control amplitude A_H, namely, nonmonotonic behavior with a passing through the maximum, a broadening of the response curves, and a shift and rise of the maximal value of R_L as the LF amplitude increases. However, there are some differences between the uses of different types of signals. The response amplitude R_L in the case of a square-wave signal is almost three times higher than for a sine-wave signal. In addition, the shapes of the response curves for square-wave signals are more narrow. Such a difference is a consequence of the probabilistic character of the response of the SPAD. Figures 4(b) and 4(d) give an idea about the response at the frequency f_H of the control HF signal.

One of the peculiarities is very different dependencies of the response R_L on the amplitude of the LF signal A_L for sine-wave and square-wave input signals shown in Fig. 5. In all these measurements the total value of the amplitudes of the periodic signals is held to less than 2.25 V in order to prevent damage to the laser diode. That is why each curve in Fig. 4 finishes for different values of the amplitude A_H.

V. SIGNAL-TO-NOISE RATIO

The signal-to-noise ratio is one of the major characteristics in the detection of weak signals which determines the resulting reliability of the signal characteristics measurement. Figure 6 demonstrates the results of the SNR evaluation for both sinusoidal and rectangular shapes of the signals obtained for different values of the LF amplitude. The SNR is defined here for both types of the signals as $\mathrm{SNR} = S(f_L)/S_N(f_L)$, where $S(f_L)$ and $S_N(f_L)$ are the response of the system to the effect of the LF signal and the noise background at a frequency f_L, respectively, which were evaluated from the amplitude spectra of the Fourier-transformed time series. One can see the strong rise of the SNR with respect to the initial values as the amplitude A_H increases up to the optimal values A_H corresponding to maximal responses R_L. Thus, these results

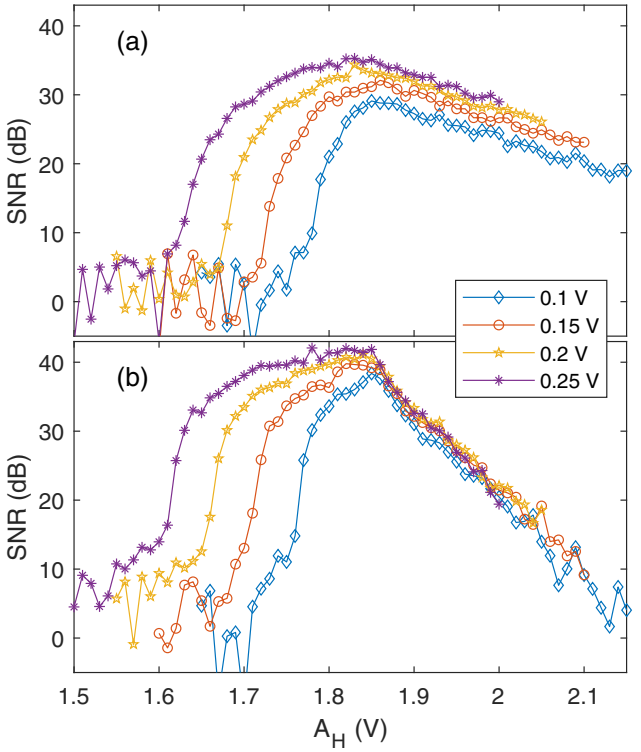

FIG. 6. SNR as a function of the HF amplitude A_H for (a) sine-wave and (b) square-wave LF signals shown for different values of the LF amplitude depicted in the inset.

demonstrate that the signal amplification and the SNR gain for both types of periodic signals can be obtained simultaneously in the ASN.

VI. INTERSPIKE INTERVALS DISTRIBUTION

As shown Figs. 1 and 2, the temporal responses of the ASN have a series of spikes with a rather stochastic character especially far from the optimal amplitude of the HF signal. This is due to a probabilistic character of the ASN response to the effect of the low-intensity laser pulses with a duration significantly larger than the SPAD deadtime. Therefore we studied the evolution of interspike intervals (ISIs) depending on the amplitude of the additional HF modulation. ISIs are widely used in neuroscience for a characterization of the spike time variability in neurons with noise [35]. Here, ISIs are obtained from the time series of pulses reduced to a δ-spike sequence. The interspike interval T is the time interval between two successive δ spikes. Such a reduction was performed by the program after acquiring and digitizing the signals by a USB oscilloscope. The procedure of the data processing was as follows. We set a threshold equal to half of the amplitude of pulses from SPAD. Then we apply a signum function to the data. After differentiation of a series of rectangular pulses, we obtain a sign-alternating series of delta pulses. Then we find the indices of all positive delta pulses. After differentiation of the array of indices we obtain an array of interspike intervals. Figure 7 shows a histogram of interspike intervals obtained for different values of the amplitude HF signal. One can see that the distribution has a complex

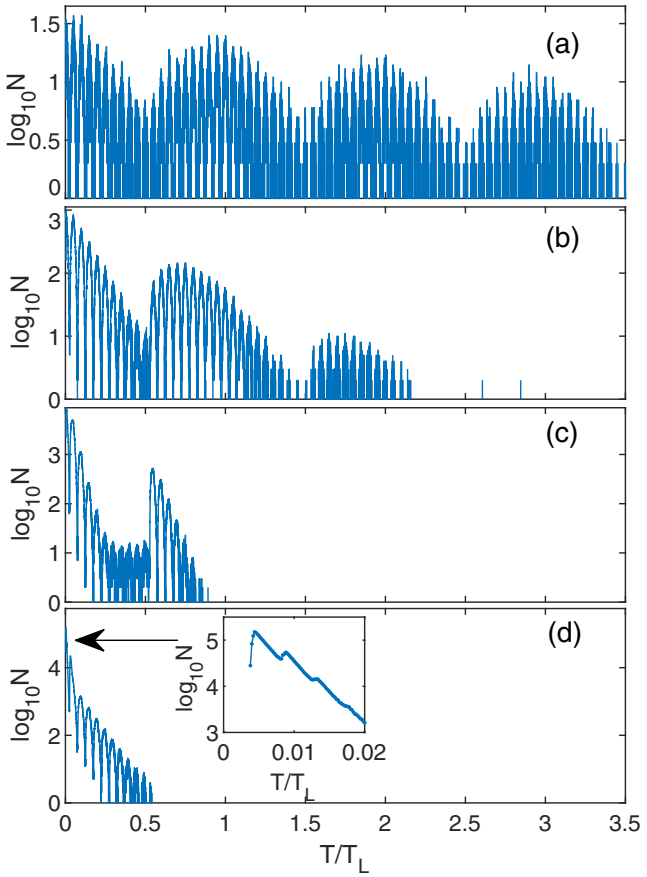

FIG. 7. (a) Distributions of interspike intervals T as a function of time, normalized by the period of the LF signal T_L shown for different values of (a) $A_H = 1.66$, (b) 1.67, (c) 1.67, and (d) 1.89 V. The amplitude of the LF signal $A_L = 0.2$ V. Both LF and HF signals have square-wave shapes. N is a number of intervals in the stated time bin.

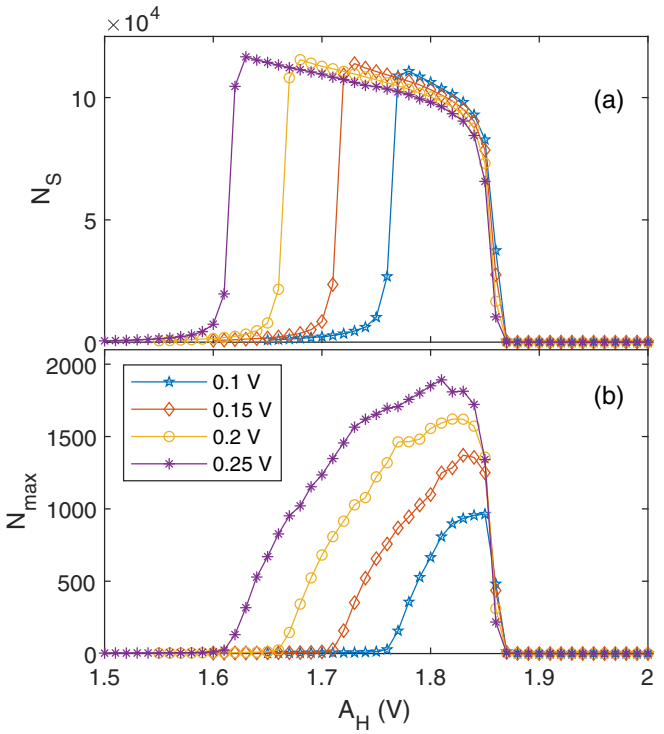

FIG. 8. Area under the peak N_S and the maximal amplitude $N_{\max}$ in this area as a function of the HF control amplitude for sine-wave signals.

multimodal structure. This is a consequence of the probabilistic character of the SPAD responses for low-intensity laser pulses in the case of biperiodic modulation signals. The low-frequency shape in the histogram in Fig. 7(a) corresponds to the effect of the LF input signal where the maxima appear with a period T_L of the LF signal. At the same time each LF period in the histogram in the range of $t \in [nT_L - T_L/2, nT_L + T_L/2]$ $(n = 1, 2, \ldots)$ consists of 20 distributions caused by the effect of the HF signal. As the amplitude A_H increases one can note a deformation of histograms and a disappearance of intervals larger than T_L [Figs. 7(c) and 7(d)]. One can note also for the short time less the deadtime there are no interspike intervals. It can be seen from the inset in Fig. 7(d). A similar picture is observed for all distributions presented in Fig. 7.

One of the indicators widely used for the characterization of the phenomenon of stochastic resonance is an area under the first peak in the resident time distribution of interspike intervals [36]. We introduce here the area N_S under the region from $T_L - T_L/2$ to $T_L + T_L/2$ and its maximal amplitude $N_{\max}$ in the interspike interval distribution as indicators for VR in the ASN with a probabilistic character of the responses. This area N_S centered at T_L (integrated from $T_L - T_L/2$ to $T_L + T_L/2$ or from 0.5 to 1.5 in normalized form) is shown in Fig. 8(a) while the maximal amplitude $N_{\max}$ is presented in Fig. 8(b) as a function of the amplitude of the HF signal at fixed values of the amplitude A_L. One can see that both indicators pass through the maximum as a function of the amplitude A_H though the shape of the curves are different. An increase of the amplitude A_L results in a decrease of the optimal value of the control amplitude A_H which are different for both indicators.

VII. CONCLUSIONS

To conclude, we have presented experimental evidence of the phenomenon of VR in an optoelectronic artificial spiking neuron based on a single photon avalanche diode and a VCSEL. The phenomenon of VR manifests itself as a strong amplification of very weak subthreshold sine-wave and square-wave periodic signals at an optimal amplitude of the additional HF modulation with the simultaneous rise of the SNR leading to an improvement of the signal propagation through the artificial spiking neuron. These results can be important from the standpoint of the control of the information transfer in spiking neural networks based on artificial spiking neurons. We believe that the phenomenon of VR can be observed with other types of artificial spiking neurons based on other physical principles [37].

[1] P. S. Landa and P. V. E. McClintock, Vibrational resonance, J. Phys. A: Math. Gen. **33**, L433 (2000).

[2] R. Benzi, A. Sutera, and A. Vulpiani, The mechanism of stochastic resonance, J. Phys. A: Math. Gen. **14**, L453 (1981).

[3] L. Gammaitoni, P. Hänggi, P. Jung, and F. Marchesoni, Stochastic resonance, Rev. Mod. Phys. **70**, 223 (1998).

[4] A. A. Zaikin, L. López, J. P. Baltanás, J. Kurths, and M. A. F. Sanjuán, Vibrational resonance in a noise-induced structure, Phys. Rev. E **66**, 011106 (2002).

[5] E. Ullner, A. Zaikin, J. García-Ojalvo, R. Bóscones, and J. Kurths, Vibrational resonance and vibrational propagation in excitable systems, Phys. Lett. A **312**, 348 (2003).

[6] J. P. Baltanás, L. López, I. I. Blechman, P. S. Landa, A. Zaikin, J. Kurths, and M. A. F. Sanjuán, Experimental evidence, numerics, and theory of vibrational resonance in bistable systems, Phys. Rev. E **67**, 066119 (2003).

[7] V. N. Chizhevsky, E. Smeu, and G. Giacomelli, Experimental evidence of "vibrational resonance" in an optical system, Phys. Rev. Lett. **91**, 220602 (2003).

[8] V. N. Chizhevsky and G. Giacomelli, Experimental and theoretical study of vibrational resonance in a bistable system with asymmetry, Phys. Rev. E **73**, 022103 (2006).

[9] A. Wickenbrock, P. C. Holz, N. A. Abdul Wahab, P. Phoonthong, D. Cubero, and F. Renzoni, Vibrational mechanics in an optical lattice: Controlling transport via potential renormalization, Phys. Rev. Lett. **108**, 020603 (2012).

[10] A. Abusoua and M. F. Daqaq, Experimental evidence of vibrational resonance in a mechanical bistable twin-well oscillator, J. Comput. Nonlinear Dyn. **13**, 061002 (2018).

[11] A. Chowdhury, M. G. Clerc, S. Barbay, I. Robert-Philip, and R. Braive, Weak signal enhancement by nonlinear resonance control in a forced nano-electromechanical resonator, Nat. Commun. **11**, 2400 (2020).

[12] G. Madiot, S. Barbay, and R. Braive, Vibrational resonance amplification in a thermo-optic optomechanical nanocavity, Nano Lett. **21**, 8311 (2021).

[13] K. Abirami, S. Rajasekar, and M. A. F. Sanjuan, Vibrational resonance in the Morse oscillator, Pramana **81**, 127 (2013).

[14] O. I. Olusola, O. P. Shomotun, U. E. Vincent, and P. V. E. McClintock, Quantum vibrational resonance in a dual-frequency-driven Tietz-Hua quantum well, Phys. Rev. E **101**, 052216 (2020).

[15] P. Sarkar, S. Paul, and D. S. Ray, Subharmonics and superharmonics of the weak field in a driven two-level quantum system: Vibrational resonance enhancement, Phys. Rev. E **104**, 014202 (2021).

[16] K. Omoteso, T. Roy-Layinde, J. Laoye, U. Vincent, and P. McClintock, Acoustic vibrational resonance in a Rayleigh-Plesset bubble oscillator, Ultrason. Sonochem. **70**, 105346 (2021).

[17] K. Oyeleke, O. Olusola, U. Vincent, D. Ghosh, and P. McClintock, Parametric vibrational resonance in a gyroscope driven by dual-frequency forces, Phys. Lett. A **387**, 127040 (2021).

[18] C. Jeevarathinam, S. Rajasekar, and M. A. F. Sanjuán, Vibrational resonance in groundwater-dependent plant ecosystems, Ecol. Complex. **15**, 33 (2013).

[19] S. Rajasekar and M. A. F. Sanjuán, Vibrational resonance in time-delayed nonlinear systems, in *Nonlinear Dynamics and Complexity*, edited by V. Afraimovich, A. C. J. Luo, and X. Fu (Springer International, Cham, 2014), pp. 235–260.

[20] M. Gosak, M. Perc, and S. Kralj, The impact of static disorder on vibrational resonance in a ferroelectric liquid crystal, Mol. Cryst. Liq. Cryst. **553**, 13 (2012).

[21] S. Morfu, B. I. Usama, and P. Marqui, On some applications of vibrational resonance on noisy image perception: The role of the perturbation parameters, Philos. Trans. R. Soc. A **379**, 20200240 (2021).

[22] Z.-X. Zhou, K.-L. Yang, C.-J. Wang, B. Yu, X.-B. Li, and Y.-W. Su, Theory and numerics of vibrational resonance in a three-level atomic optical bistable system, Chaos, Solitons Fractals **170**, 113355 (2023).

[23] M. Perc and M. Marhl, Amplification of information transfer in excitable systems that reside in a steady state near a bifurcation point to complex oscillatory behavior, Phys. Rev. E **71**, 026229 (2005).

[24] B. Deng, J. Wang, X. Wei, K. M. Tsang, and W. L. Chan, Vibrational resonance in neuron populations, Chaos **20**, 013113 (2010).

[25] L. Yang, W. Liu, M. Yi, C. Wang, Q. Zhu, X. Zhan, and Y. Jia, Vibrational resonance induced by transition of phase-locking modes in excitable systems, Phys. Rev. E **86**, 016209 (2012).

[26] Y. Qin, J. Wang, C. Men, B. Deng, and X. Wei, Vibrational resonance in feedforward network, Chaos **21**, 023133 (2011).

[27] Y. Qin, C. Han, Y. Che, and J. Zhao, Vibrational resonance in a randomly connected neural network, Cogn. Neurodyn. **12**, 509 (2018).

[28] V. Baysal and E. Yilmaz, Effects of electromagnetic induction on vibrational resonance in single neurons and neuronal networks, Physica A **537**, 122733 (2020).

[29] G. Wang, D. Yu, Q. Ding, T. Li, and Y. Jia, Effects of electric field on multiple vibrational resonances in hindmarsh-rose neuronal systems, Chaos, Solitons Fractals **150**, 111210 (2021).

[30] M. Bordet and S. Morfu, Experimental and numerical enhancement of vibrational resonance in neural circuit, Electron. Lett. **48**, 903 (2012).

[31] M. Bordet and S. Morfu, Experimental and numerical study of noise effects in a FitzHugh-Nagumo system driven by a biharmonic signal, Chaos, Solitons Fractals **54**, 82 (2013).

[32] M. Bordet, S. Morfu, M. Rosse, and P. Marquie, Propagation enhancement in neural network, Electron. Lett. **51**, 1482 (2015).

[33] S. Morfu and M. Bordet, On the propagation of a low frequency excitation in a perturbed FitzHugh-Nagumo system: Simulation and experiments, Chaos, Solitons Fractals **103**, 205 (2017).

[34] V. N. Chizhevsky, V. A. Kulchitsky, and S. Y. Kilin, Artificial spiking neuron based on a single-photon avalanche diode and a microcavity laser, Appl. Phys. Lett. **119**, 041107 (2021).

[35] W. Gerstner, W. M. Kistler, R. Naud, and L. Paninski, *Neuronal Dynamics: From Single Neurons to Networks and Models of Cognition* (Cambridge University Press, Cambridge, UK, 2014).

[36] M. H. Choi, R. F. Fox, and P. Jung, Quantifying stochastic resonance in bistable systems: Response vs residence-time distribution functions, Phys. Rev. E **57**, 6335 (1998).

[37] J. Zhu, T. Zhang, Y. Yang, and R. Huang, A comprehensive review on emerging artificial neuromorphic devices, Appl. Phys. Rev. **7**, 011312 (2020).